Journal of Alloys and Compounds 509 (2011) 5962–5968

Contents lists available at ScienceDirect

Journal of Alloys and Compounds

journal homepage: www.elsevier.com/locate/jallcom

Optical and electrical properties of zinc oxide thin films with low resistivity via Li–N dual-acceptor doping

Daoli Zhang[a,b,*], Jianbing Zhang[a,b], Zhe Guo[a], Xiangshui Miao[a,b]

[a] Department of Electronic Science and Technology, Huazhong University of Science and Technology, No. 1037 Luoyu Road, Hongshan District, Wuhan City, Hubei Province 430074, PR China

[b] Wuhan National Laboratory for Optoelectronics, 1037 Luoyu Road, Hongshan District, Wuhan City, Hubei Province 430074, PR China

ARTICLE INFO

Article history:
Received 30 November 2010
Received in revised form 24 February 2011
Accepted 6 March 2011
Available online 11 March 2011

PACS:
71.20.Nr
61.46.Hk
61.72.dd

Keywords:
Ultraviolet emission
Electronic properties
Li–N dual-acceptor doping
Zinc oxide thin films
Successive ionic layer adsorption and reaction

ABSTRACT

Zinc oxide thin films with low resistivity have been deposited on glass substrates by Li–N dual-acceptor doping method via a modified successive ionic layer adsorption and reaction process. The thin films were systematically characterized via scanning electron microscopy (SEM), atomic force microscopy (AFM), X-ray diffraction, ultraviolet-visible spectrophotometry and fluorescence spectrophotometry. The resistivity of zinc oxide film was found to be 1.04 Ω cm with a Hall mobility of 0.749 $cm^2 V^{-1} s^{-1}$ and carrier concentration of 8.02×10^{18} cm^{-3}. The Li–N dual-acceptor doped zinc oxide films showed good crystallinity with prior *c*-axis orientation, and high transmittance of about 80% in visible range. Moreover, the effects of Li doping level and other parameters on crystallinity, electrical and ultraviolet emission of zinc oxide films were investigated.

1. Introduction

As an *n*-type compound semiconductor with a hexagonal wurtzite structure, zinc oxide has attracted considerable attention for its wide band gap (3.37 eV), large exciton binding energy (60 meV) and high carrier mobility at room temperature [1]. It has exhibited enormous potential in many electronic device applications, such as light emitting diodes [2], ultraviolet (UV) lasers [3], transparent thin film transistors [4], gas sensors [5], and surface acoustic devices [6]. However, the bottleneck of preparing zinc oxide films with p-type conductivity should be overcome before zinc oxide could make inroads into the world of electronics devices [7]. Normally, undoped zinc oxide shows n-type conductivity due to the native donor defects such as zinc interstitial and oxygen vacancy, which makes it difficult to prepare p-type conductive zinc oxide [8]. Even so, considerable efforts have been made in this field, for example, p-type zinc oxide have been made employing N [9,10], P [11], As [12], Li and Ag [13] as dopants. Based on the theory of co-doping, In–P [11] and Al–N [14] co-doping methods were introduced into the fabrication of p-type zinc oxide.

Up to now, many existing thin film preparation techniques have been applied in the synthesis of zinc oxide films, including chemical vapor deposition [9], sputtering [12], pulsed laser deposition [15], molecular beam epitaxy [16], sol–gel techniques [17], chemical bath deposition [18], successive ionic layer adsorption and reaction (SILAR) [19–25], et al. However, it is well conceived that preparation of zinc oxide films via solution chemical routes provides a promising option for large-scale production of zinc oxide materials. SILAR method, first reported by Nicolau in 1985, involves the substrate alternate immersion in cationic and anionic precursor and the substrate rinsing procedures in between. It has attracted much interest because of low-cost and environment-friendly circumstance. Films prepared by this method have good adhesion and uniformity, and the thickness of the film can easily be controlled by changing cycle number, pH value, and other technical parameters. The SILAR method has been used to prepare zinc, lead and cadmium chalcogenide thin films.

In the previous work, we reported the synthesis and ultraviolet emission of un-doped zinc oxide polycrystalline films by a modi-

* Corresponding author at: Department of Electronic Science and Technology, Huazhong University of Science and Technology, No. 1037 Luoyu Road, Hongshan District, Wuhan City, Hubei Province 430074, PR China. Tel.: +86 27 87542894; fax: +86 27 87542693.
E-mail address: zhang_daoli@mail.hust.edu.cn (D. Zhang).

0925-8388/$ – see front matter © 2011 Elsevier B.V. All rights reserved.
doi:10.1016/j.jallcom.2011.03.028

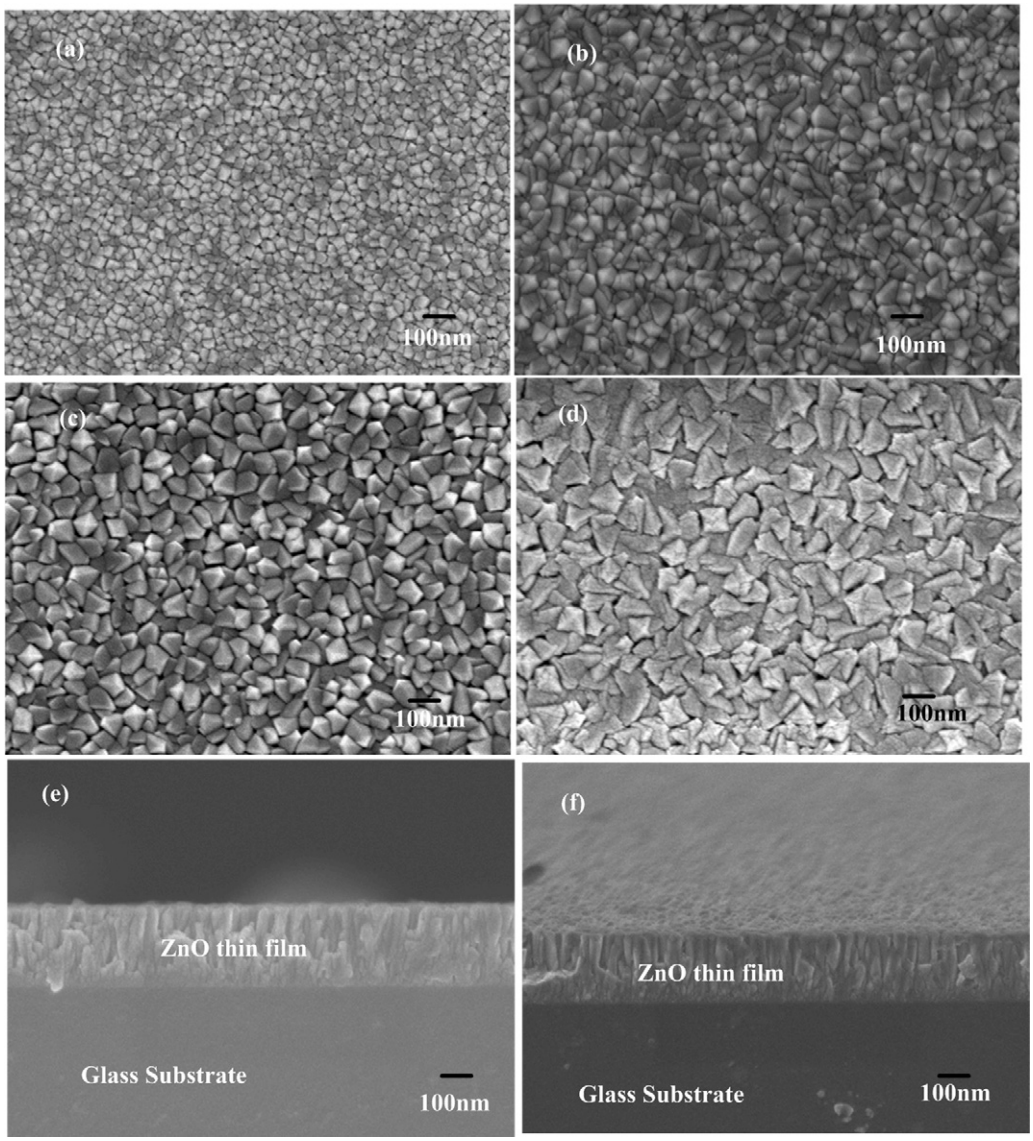

Fig. 1. SEM images of ZnO:Li_0 films without heat treatment process and with heat treatment at different temperatures in O_2 atmosphere for 2 h. (a) As-deposited ZnO film; (b) annealed at 350 °C; (c) annealed at 450 °C; (d) annealed at 530 °C; (e) as-deposited ZnO film; (f) annealed 530 °C.

fied SILAR method [21]. In this paper, stable zinc oxide thin films with low resistivity were fabricated by a Li–N dual-acceptor doping technique via the modified SILAR method. A heat treatment process was introduced in the present work, and the as-prepared zinc oxide films have good crystallinity, electrical and ultraviolet emission properties.

2. Experimental procedure

2.1. Treatment of glass substrates

The cleanness and hydrophilicity of substrates are very important to the deposition of high-quality zinc oxide films. Contaminated substrates will lead to formation of non-uniform films. In the present work, commercially obtained glass slides with dimensions of 25 mm × 75 mm × 1 mm were chosen as substrates. The substrates were cleaned by detergent and treated with hydrogen nitrate or chromic acid for 12 h, followed by ultrasonic cleaning in deionized water for 30 min and then drying.

2.2. Formation of zinc oxide thin films with low resistivity

A series of zinc oxide films with different Li contents were deposited on cleaned glass substrates. The cationic precursor of SILAR process was prepared as the following: 0.02 mol ethanolamine and 15 mL 6.65 mol L^{-1} ammonia solutions were added to 100 mL 0.2 mol L^{-1} zinc acetate solution, and then the solution was diluted to 200 mL with deionized water. Lithium nitrate, as lithium dopant, was also added to the solution. Lithium contents of 0, 0.1, 0.5, 1, 2, 5 and 10 at.% were employed in this study, and the zinc oxide films grown with these Li contents will be referred to as ZnO:Li_0, ZnO:$Li_{0.001}$, ZnO:$Li_{0.005}$, ZnO:$Li_{0.01}$, ZnO:$Li_{0.02}$, ZnO:$Li_{0.05}$ and ZnO:$Li_{0.1}$, respectively. Generally, the lithium doped levels in the films are not equal to the lithium contents in the solutions. The pH value of the cationic precursor was maintained at ~11.5. The ethanolamine was used to reduce the dosage of ammonia as a high ammonia concentration may result in dissolution of as-deposited zinc oxide films when being reintroduced into the cationic precursor [22]. Moreover, both ethanolamine and ammonia can be used as the N-doping source. Hot water of 90 °C was used as anionic precursor to provide hydroxyl anions during the fabrication of zinc oxide films.

A complete film deposition cycle involves four steps: (i) immersion of the substrate in cationic precursor at room temperature for 30 s, after which there will be a thin layer solution adhered to the substrate surface, (ii) immersion of the substrate in anionic precursor at 90 °C for 30 s, which leads to the chemical reaction on the substrate surface, (iii) water rinsing of the loosely bound particles, and (iv) heat treatment of the as-prepared films at 200 °C for 5 min to convert zinc hydroxide into zinc oxide. All samples in this paper were prepared with 15 deposition cycles. After the deposition, zinc oxide films were annealed in different ambient (O_2, N_2 and air) for comparison. Annealing process includes a preheating step at 300 °C for an hour to vaporize organic ingredients, and a post-heating step at different temperatures

such as 350 °C, 450 °C, and 530 °C for 2 h to improve the crystallinity of the thin films.

2.3. Characterization of zinc oxide thin films

The surface morphologies of ZnO thin films were characterized and analyzed by scanning electron microscopy (SEM, JEOL JEM-6700F at 3.0 kV), and atomic force microscope (AFM, Digital Instruments, Dimension 3000 Nanoscope). AFM scanned area is 1 μm × 1 μm. The crystalline structure of the samples were identified with X-ray diffraction (XRD) using a PANalytical X'Pert PRO diffractometer, in which Cu Kα radiation with a wavelength of 0.154 nm was employed as the X-ray source. For electrical characterization, Hall-effect measurements were carried out in the Van der Pauw configuration (Accent HL5500PC) at room temperature. The *I–V* and *I–R* curves obtained via four point probe method were used to evaluate the ohmic contact of the samples. The transmission properties were measured by ultraviolet-visible spectrophotometer (Shimadzu UV-2550), and room temperature photoluminescence (PL) spectra of the films were measured by a fluorescent spectrometer (Jasco FP-6500) with He–Cd laser (λ_{ex} = 330 nm) as the excitation source.

3. Results and discussion

3.1. Microstructure of zinc oxide thin films with low resistivity

Fig. 1(a)–(d) shows the SEM images of ZnO:Li_0 thin films unannealed and annealed at different temperatures in O_2 atmosphere for 2 h. The surface of the films are smooth and consisted of uniformly distributed octahedral grains without any pinholes or islands. The films annealed at lower temperatures exhibit inhomogeneous size distributions from a few nanometers to about ~100 nm. Moreover, the grain sizes become bigger and more uniform with the increase of the annealing temperature.

Fig. 1(e) and (f) display the cross-section SEM view of ZnO:Li_0 films with and without heat treatment process. The films without heat treatment consisted of compacted pillar crystals with an average height of ~250 nm, while the average height decreased to ~200 nm after the film was treated at 530 °C in O_2 atmosphere for 2 h.

Fig. 2 shows three-dimensional AFM images of ZnO:Li_0 films with and without heat treatment process. The root mean-square (RMS) roughness of the unannealed film was 9.69 nm while it decreased to 6.91 nm for the film annealed at 530 °C in O_2 atmosphere for 2 h. This indicates that heat treatment process contributed to formation of smooth surface. In addition, the grains in the annealed film were packed much closer than those in the unannealed film. The reason for this behaviour is that the mobility of the absorbed atoms is controlled by heat treatment process. The as-deposited ZnO thin films should tend to form crystallite structure with highly porous and rough surface due to lower mobility of the absorbed atoms. However, the mobility of surface atoms is enhanced after being treated at 530 °C. Due to the higher surface mobility, more atoms will be able to reach crystalline regions, which results in a smoother surface and large grains without discernible boundaries.

The crystallinity of zinc oxide films was influenced by the heat treatment process dramatically. Fig. 3 shows the significant change in crystallinity of zinc oxide films due to heat treatment. XRD patterns of the two samples indicate both the films with and without heat treatment possess hexagonal wurtzite structure. The positions and relative intensities of the three dominant peaks of the sample without heat treatment match well with the standard XRD pattern of bulk zinc oxide (JCPDS: No 79-2205). The heat-treated films showed a highly *c*-axis preferential orientation, which is in accordance with the fact that heat treatment contributes to the improvement of *c*-axis orientation.

All samples with heat treatment show good crystallinity and highly preferential *c*-axis orientation, as shown in Figs. 4 and 5. However, Li content and the annealing temperature also affect the growth orientation. After 350 °C annealing, *c*-axis orientation becomes weaker, which was also reported by Jiménez-González

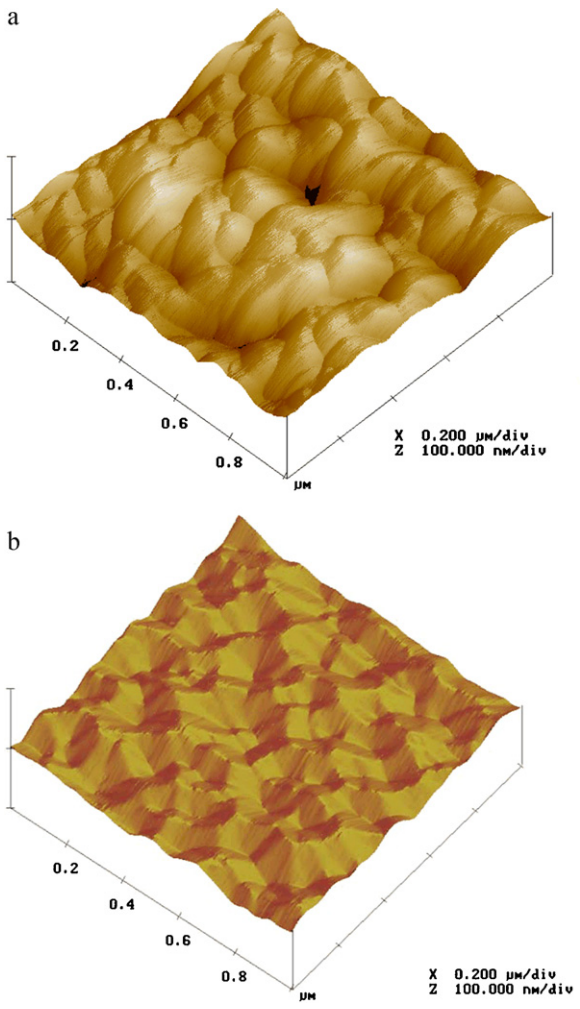

Fig. 2. Three-dimensional AFM images of ZnO:Li_0 films with and without heat treatment process. (a) As-deposited ZnO film; (b) annealed at 530 °C. AFM scanned area is 1 μm × 1 μm.

[23,24]. Given that (1 0 0), (1 2 0) and (0 0 1) facets have lower energy, these orientation may be formed more easily during recrystallization [1]. Furthermore, other facets which have higher energy than (0 0 1) facet would be developed with enough thermal energy [15]. But films annealed at 450 °C and 530 °C show better *c*-axis orientation, revealing that crystallinity is improved at a higher annealing temperature. Grain sizes, calculated using

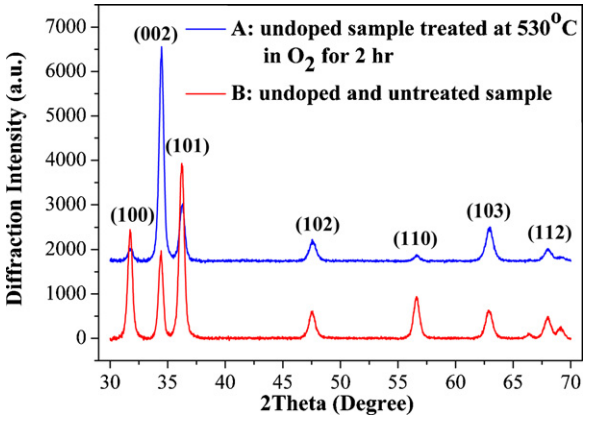

Fig. 3. XRD patterns of ZnO:Li_0 films with and without heat treatment process.

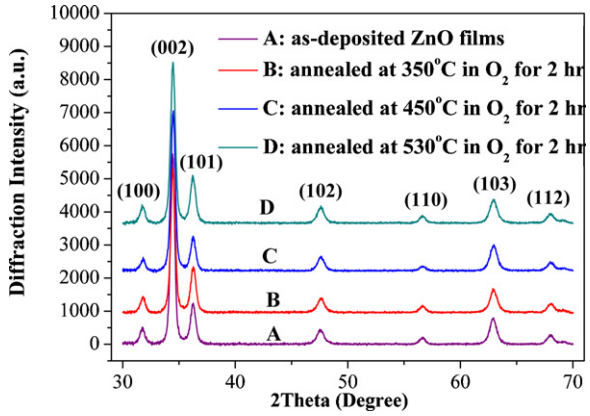

Fig. 4. XRD patterns of ZnO:$Li_{0.05}$ films annealed at different temperature.

Debye–Scherrer formula, of the four samples in Fig. 4 are 18.8, 17.5, 17.1 and 17.0 nm, respectively. The decrease of the grain size should be ascribed to recrystallization. No diffraction from other phases such as Li_2O is detected in Fig. 5, suggesting that Li is doped in zinc oxide without formation of other compound. Obviously ZnO:$Li_{0.02}$ has the best (0 0 2) orientation of the four samples in Fig. 5, indicating that there is an optimum Li content providing preferred crystal orientation. The degrading crystallinity was attributed to incorporation of Li atoms [11]. In fact, zinc oxide films would not grow from a cationic precursor with Li content of 15 at.%, and the reason is not very clear yet.

Peak positions of all samples in Figs. 4 and 5 are almost identical, indicating that the films have the same lattice constants. The *d* values were calculated using the Bragg law, and then lattice constants *a*, *c* of hexagonal could be evaluated, which are 3.25 and 5.20 Å on average, respectively. The c constant is a little smaller than that of bulk zinc oxide, arising from the difference in ionic radii between the host Zn (0.074 nm) and doped Li (0.060 nm) [12].

3.2. Electronic properties of zinc oxide thin films with low resistivity

As indicated in Fig. 6, and Table 1, only ZnO:$Li_{0.05}$ annealed in O_2 atmosphere at 530 °C exhibits definitive p-type conductivity, with a resistivity of 1.04 Ω cm, Hall mobility of 0.75 $cm^2/V\,s$, and hole concentration of 8.02×10^{18} cm^{-3}, comparable with those dates reported by Tetsuya [14]. In the presence of donor defects, ZnO:(Li,N) exhibits two-band mixed conduction, and the current,

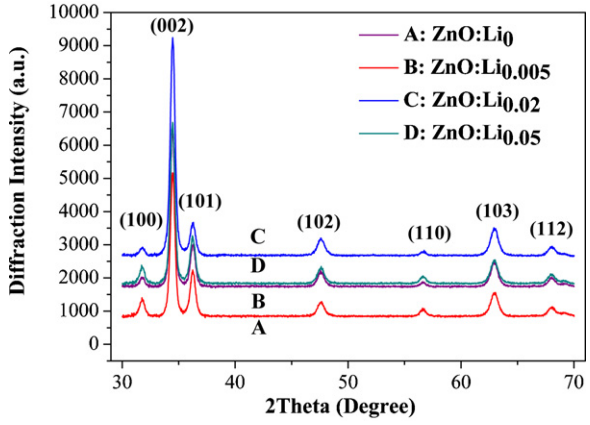

Fig. 5. XRD patterns of zinc oxide films prepared with different Li contents and annealed in O_2 at 530 °C.

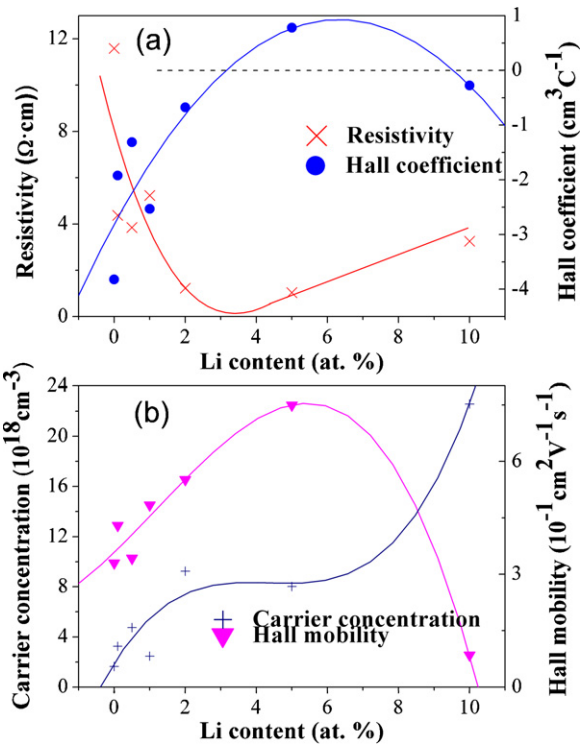

Fig. 6. (a) Resistivity and Hall coefficient of ZnO:(Li,N) films as a function of Li contents. (b) Carrier concentration and Hall mobility of ZnO:(Li,N) films as a function of Li contents.

conductivity, and Hall coefficient take the form [8]

$$j_x = j_{px} + j_{nx} \tag{1}$$

$$\sigma = \sigma_p + \sigma_n = e(p\mu_p + n\mu_n) \tag{2}$$

$$R_H = \frac{R_p\sigma_p^2 + R_n\sigma_n^2}{(\sigma_p + \sigma_n)^2} = \frac{p\mu_p^2 - n\mu_n^2}{e(p\mu_p + n\mu_n)^2} \tag{3}$$

The type of conductivity is determined by the sign of R_H, which would go to zero when the numerator in (3) became zero. Li and N doping of zinc oxide would introduce Li_{Zn} and N_O substitution, both of which are acceptor defects. So the concentration of holes would increase with the increase of Li contents. As a result, R_H decreases and its sign become positive when the Li content reaches 5 at.%. Namely, the inversion of the conductivity type occurred. The curve of Hall coefficient in Fig. 6 reveals this tendency, while the segment above the dash line exhibits p-type conductivity. Interstitial Li atoms as donor defects may account for the second inversion that took place at a higher Li content. Note that Li_{Zn} has a larger possibility to be formed than Li_i, numerous interstitial Li atoms would only be formed at high Li contents [12]. It is known that impurity scattering would reduce the mobility. Therefore, Hall mobility decreases at high Li contents, as more defects are introduced. That is the reason why the resistivity of zinc oxide films increases when Li content reaches 10 at.%, as shown in Fig. 6.

For comparison, ZnO:(Li,N) films were also prepared. It is shown in Table 1 that the resistivity of ZnO:(Li,N) films annealed in N_2 atmosphere at 530 °C is 20 times larger than that of ZnO:(Li,N) films annealed in O_2 atmosphere at 530 °C, despite of the Li contents. All samples annealed in N_2 atmosphere exhibit definitive n-type conductivity. This is presumably due to the compensation of oxygen vacancies in an oxygen-rich condition. With the same ambience, ZnO:$Li_{0.05}$ annealed at 530 °C shows much lower resistivity than ZnO:$Li_{0.05}$ annealed at 450 °C. Moreover, ZnO:$Li_{0.05}$ annealed at 530 °C shows p-type conductivity, while the other shows n-type

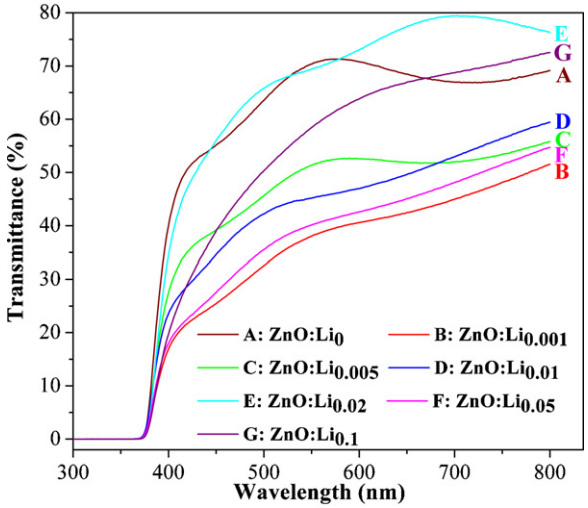

Fig. 7. Optical transmittance spectra of zinc oxide films annealed in O_2 at 530 °C with different Li contents.

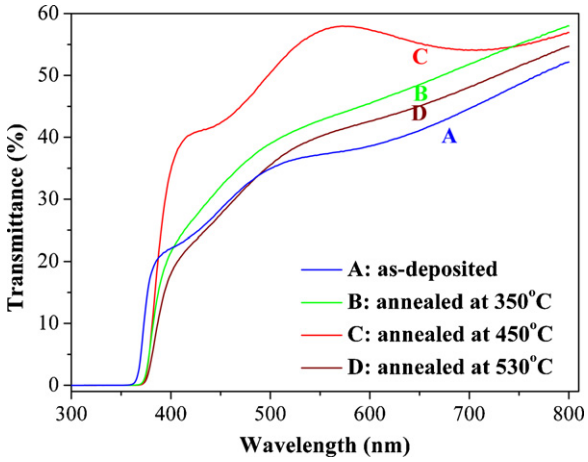

Fig. 8. Optical transmittance spectra of $ZnO:Li_{0.05}$ films annealed in O_2 at different temperatures.

conductivity. These results evidently demonstrate that annealing at a high temperature would improve incorporation of Li in zinc oxide films. In addition, it should be noticed that annealing at 530 °C would significantly reduce the concentration of hydrogen, which plays a role of donor in the films, while nitrogen concentration would remain constant at such a high temperature [5].

3.3. Optical properties of synthesized ZnO thin films with low resistivity

The optical transmittance spectra are given in Figs. 7 and 8. It is found that the transmittance of the samples is related to *c*-axis orientation of zinc oxide films. Zinc oxide films with a highly *c*-axis

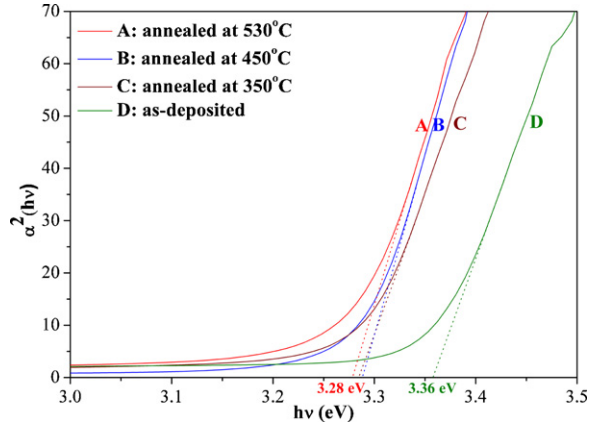

Fig. 9. The $\alpha^2(h\nu)$ versus $h\nu$ curves for the optical band gap determination in $ZnO:Li_{0.05}$ films annealed at different temperatures.

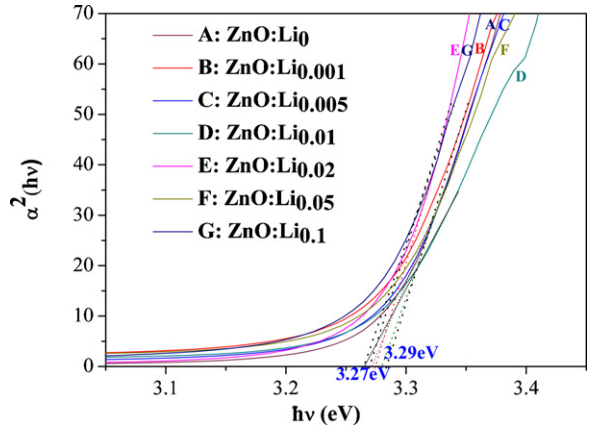

Fig. 10. $\alpha^2(h\nu)$ versus $h\nu$ curves for zinc oxide films with different Li contents.

preferential orientation show a high transmittance. $ZnO:Li_{0.02}$ films have the highest transmittance of about 80% in part of the visible region. Zinc oxide films without heat treatment process are nearly opaque, and the data was not shown here. Annealed zinc oxide films show higher transmittance than as-deposited zinc oxide, as shown in Fig. 8.

An analysis of the optical band gap (E_g) of zinc oxide films was made using the optical absorption coefficient (α) in the $\alpha^2(h\nu)$ versus $h\nu$ plot, where h is the Planck constant and ν the frequency. As shown in Fig. 9, the band gap (E_g) of zinc oxide films decreases from 3.36 eV to 3.28 eV with the increase of annealing temperature. The tendency was also reported by Kang and Jiménez-González [15,23]. The shift of band gap energy is related to the structural property. The annealing treatment would reduce the grain size of ZnO, as concluded from XRD patterns, indicating the relaxation of the tensile build-in strain in zinc oxide films. Annealing treatment would provide sufficient thermal energy for the relaxation, which could account for the shift of band gap energy [15]. Figs. 10 and 11

Table 1
Electrical properties of ZnO:(Li,N) films prepared in different annealing conditions.

Li content (at.%)	Annealing ambience	Annealing temperature (°C)	Resistivity (Ω cm)	Hall coefficient (cm^3/C)	Carrier concentration (10^{18} cm^{-3})	Hall mobility (10^{-1} cm^2/V s)	Type
5	O_2	530	1.04	0.779	8.02	7.50	p
5	N_2	530	24.9	−6.95	0.899	2.79	n
2	O_2	530	1.23	−0.676	9.24	5.51	n
2	N_2	530	27.4	−10.9	0.573	4.02	n
5	O_2	450	11.5	−0.787	7.94	0.686	n

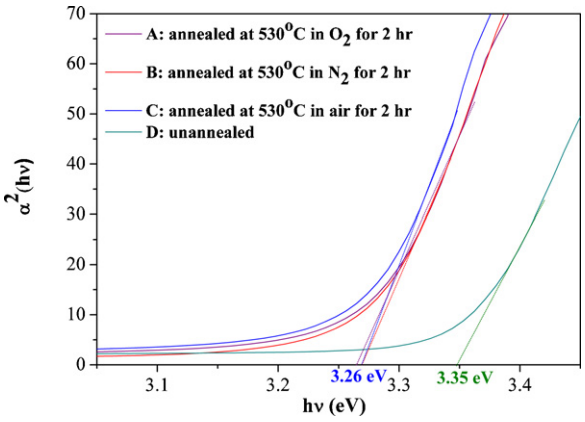

Fig. 11. $\alpha^2(h\nu)$ versus $h\nu$ curves for zinc oxide films in different annealing ambience.

show the $\alpha^2(h\nu)$ versus $h\nu$ curves for zinc oxide films with different Li contents and in different annealing ambience, and the bang gap energy of these films are in the range of 3.28–3.29 eV.

To gain more information on the Li–N dual-acceptor doping mechanism, photoluminescence measurements were performed at room temperature. Fig. 12 consists of four bands centered at 390, 411, 466, 546 nm, labeled as A, B, C, and D, respectively. A is a near-band-edge emission, while B, C, and D are deep level emission. The position of A (3.18 eV) is approximately equal to the result observed in Ye's work [26] which was ascribed to a free-to-neutral-acceptor (e, Å) transition. So band A can be assigned to a free-to-neutral-acceptor (e, Å) transition here, and the transition energy could be calculated using the following equation [26].

$$E_{eA}(T) = E_g - 60\ \text{meV} - E_A + \frac{k_B T}{2} \quad (4)$$

where $E_{eA}(T)$ is the temperature-dependent (e, Å) transition energy, E_A is the acceptor energy level, and k_B is the Boltzmann constant. Average optical band gap of 3.283 eV was considered to be E_g. Thus, the acceptor energy level is found to be 151 meV, which is equal to 150 meV reported by Ye [26]. Band D as a green luminescence band is usually associated with oxygen vacancy [27].

Band B and C could also be found in Fig. 13. Note that the intensity of band B is higher than that of band C, opposite to samples prepared with lower Li contents. The abnormality indicated that band B is related to Li interstitial. With the increase of annealing temperature, band B would have red shift, as shown in Fig. 12. As the above mentioned, annealing at a high temperature would improve the incorporation of Li in zinc oxide films. Hence, band

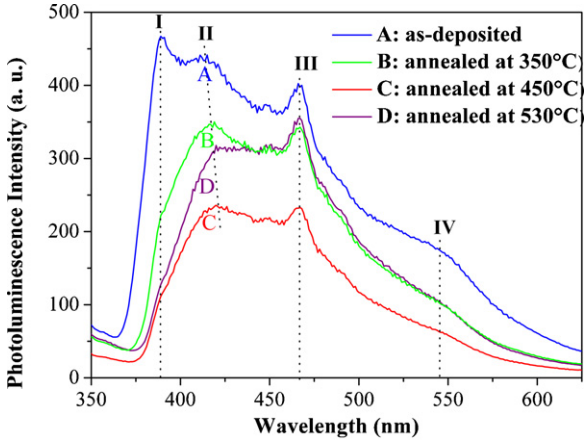

Fig. 12. Photoluminescence spectra for ZnO:$Li_{0.05}$ films annealed at different temperatures. (A) Near-band-edge emission; (B), (C), and (D) deep level emission.

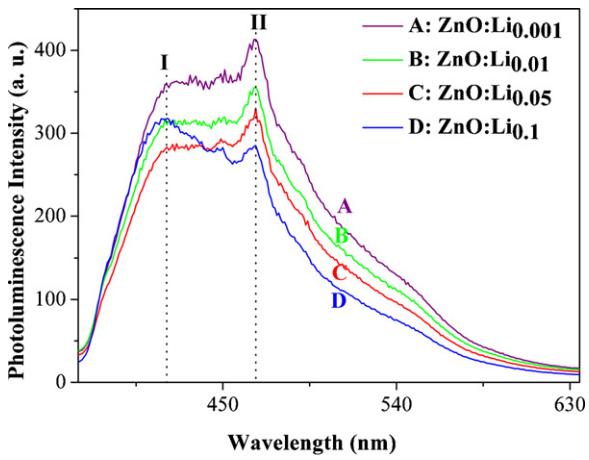

Fig. 13. Photoluminescence spectra for zinc oxide films annealed in O_2 at 530 °C with different Li contents.

B should be associated with Li_{Zn}–Li_i complex [13], with an energy level of 255 meV. Some samples with n-type conductivity attest the presence of donor energy level, which may account for band C emission.

4. Conclusions

In summary, we have demonstrated reproducible growth of Li–N dual-acceptor doped zinc oxide thin films with low resistivity by a modified SILAR method. The resistivity could be lowered to 1.04 Ω cm, with a hole concentration of 8.02×10^{18} cm^{-3}. The ZnO:(Li,N) films had high crystal quality, with prior *c*-axis orientation. Transmittance of 80% was achieved. A shallow acceptor level of 91 meV is identified from free-to-neutral-acceptor transitions. Another deep level of 255 meV was ascribed to Li_{Zn}–Li_i complex.

Acknowledgement

The authors would like to express their thanks to financial support of Hubei Provincial Natural Science Foundation (No.2007ABA048). We wish to thank the Analytical and Testing Center of Huazhong University of Science and Technology for the help on measurements.

References

[1] Z.L. Wang, J. Phys.: Condens. Matter 16 (2004) R829–R858.
[2] B. Claflin, D.C. Look, S.J. Park, G. Cantwell, J. Cryst. Growth 287 (2006) 16–22.
[3] Z.K. Tang, G.K.L. Wong, P. Yu, M. Kawasaki, A. Ohtomo, H. Koinuma, Y. Segawa, Appl. Phys. Lett. 72 (1998) 3270.
[4] H.C. Cheng, C.F. Chen, C.Y. Tsay, Appl. Phys. Lett. 90 (2007) 012113.
[5] J.F. Chang, H.H. Kuo, I.C. Leu, M.H. Hon, Sens. Actuators B: Chem. 84 (2002) 258.
[6] C.R. Gorla, N.W. Emanetoglu, S. Liang, W.E. Mayo, Y. Lu, M. Wraback, H. Shen, J. Appl. Phys. 85 (1999) 2595.
[7] Ü. Özgür, Ya I. Alivov, C. Liu, A. Teke, M.A. Reshchikov, S. Doğan, V. Avrutin, S.J. Cho, H. Morkoc, J. Appl. Phys. 98 (2005) 041301.
[8] S.B. Zhang, S.-H. Wei, A. Zunger, Phys. Rev. B: Condens. Matter. 63 (2001) 075205.
[9] J.G. Lu, S. Fujita, T. Kawaharamura, H. Nishinaka, Chem. Phys. Lett. 441 (2007) 68–71.
[10] L.L. Kerr, X. Li, M. Canepa, A.J. Sommer, Thin Solid Films 515 (2007) 5282–5286.
[11] J.D. Ye, S.L. Gu, F. Li, S.M. Zhu, R. Zhang, Y. Shi, Y.D. Zheng, X.W. Sun, G.Q. Lo, D.L. Kwong, Appl. Phys. Lett. 90 (2007) 152108.
[12] U. Wahl, E. Rita, J.G. Correia, A.C. Marques, E. Alves, J.C. Soares, Superlattices Microstruct. 42 (2007) 8–13.
[13] G.H. Kim, B.D. Ahn, D.L. Kim, K.H. Jung, S.Y. Lee, Proc. SPIE, San Jose, CA, USA, 2007, 8 pp., 647409.
[14] Y. Tetsuya, K.Y. Hiroshi, Jpn. J. Appl. Phys. 38 (1999) L166–L169.
[15] H.S. Kang, J.S. Kang, J.W. Kim, S.Y. Lee, J. Appl. Phys. 95 (2004) 1246–1250.
[16] H. Tampo, H. Shibata, P. Fons, A. Yamada, K. Matsubara, K. Iwata, K. Tamura, H. Takasu, S. Niki, J. Cryst. Growth 278 (2005) 268–272.
[17] M. Ohyama, H. Kozuka, T. Yoko, Thin Solid Films 306 (1997) 78–85.

[18] T. Saeed, P. O'Brien, Thin Solid Films 271 (1995) 35–38.
[19] Y.F. Nicolau, Appl. Surf. Sci. 22/23 (1985) 1061–1074.
[20] Y.F. Nicolau, J.C. Menard, J. Cryst. Growth 92 (1988) 128–142.
[21] D.L. Zhang, J.B. Zhang, Q.M. Wu, X.S. Miao, J. Am. Ceram. Soc. 93 (2010) 3284–3290.
[22] P. Mitra, J. Khan, Mater. Chem. Phys. 98 (2006) 279–284.
[23] A.E. Jiménez-González, R. Suárez-Parra, J. Cryst. Growth 167 (1996) 649–655.
[24] A.E. Jiménez-Gonzaílez, P.K. Nair, Semicond. Sci. Technol. 10 (1995) 1277–1282.
[25] X.D. Gao, X.M. Li, W.D. Yu, Appl. Surf. Sci. 229 (2004) 275–281.
[26] Y.J. Zeng, Z.Z. Ye, J.G. Lu, W.Z. Xu, L.P. Zhu, B.H. Zhao, Appl. Phys. Lett. 89 (2006) 042106.
[27] K. Vanheusden, C.H. Seager, W.L. Warren, D.R. Tallant, J.A. Voigt, Appl. Phys. Lett. 68 (1996) 403–405.